Insights into the mechanism of electrocatalytic CO2 reduction and concomitant catalyst degradation pathways

Raaijman, S.J.

Citation

Raaijman, S. J. (2022, January 19). *Insights into the mechanism of electrocatalytic CO2 reduction and concomitant catalyst degradation pathways*. Retrieved from https://hdl.handle.net/1887/3250500

5

Morphological stability of copper surfaces under reducing conditions

Though copper is a capable electrocatalyst for the CO_2 reduction reaction (CO2RR), it rapidly deactivates to produce mostly H_2. This has been hypothesized to occur because of potential-induced morphological restucturing leading to facet redistribution at the surface which in turn results in a shift of catalytic activity to favour H_2 formation over CO2RR. Here, we investigate the veracity of this hypothesis by studying the changes in the voltammetry of Cu(111), Cu(100), Cu(110) and polycrystalline copper after being subjected to strongly cathodic conditions. The basal planes were chosen as model catalysts, whilst polycrystalline copper served to study the overall behavior of defect-rich facets (i.e., undercoordinated sites). We found that all surfaces exhibited (perhaps surprisingly) high stability when subjected to strongly cathodic potentials in concentrated alkaline electrolyte (10 M NaOH). Proof for morphological stability under CO2RR-representative conditions (60 min at −0.75 V in 0.5 M $KHCO_3$) was obtained from identical location scanning electron microscopy, where the mesoscopic morphology for a nanoparticle-covered copper surface was found unchanged to within the instrument accuracy. Observed changes in voltammetry under such conditions, we found, were unreliable due to electrode fouling. We show that reported restructuring is likely due to oxidation, with (brief) oxidation periods (+0.50 V, 1 min) leading to changes in the facet distribution upon subsequent cathodic treatment. Therfore we posit that it is accidental oxidation/reduction cycles that are responsible for many groups observing morphological instability of copper.

5.1. Introduction

From an electrochemical perspective, the CO_2 reduction reaction (CO2RR) is a potentially lucrative pathway for the valorization of a harmful waste product: CO_2. Although catalyst selectivity and activity for this reaction are currently unfit for industrial application, many different types of functionalized carbon-containing products can be obtained via direct CO_2 reduction on e.g., copper electrodes, where > 2 electron-products are of particular interest. However, besides having sub-optimal selectivity and activity[1–5], copper is also prone to deactivation during CO2RR.[6, 7] There are various theories as to the source for this deactivation, ranging from electrode fouling by reaction products (e.g., graphitic carbon[8]) and solution impurities[6, 7], to oxidation and reduction driven surface restructuring due to strain resulting from mismatching lattice parameters[9], to evolution of surface morphology due to dissolution of surface oxides[10, 11], to cathodic corrosion (CC) [12, 13] and potential-induced surface restructuring[12, 14–17], to dissolved copper species playing an active role in the catalytic process.[18]

Of these theories, changing surface morphology under purely cathodic CO2RR conditions[12, 14, 16, 17, 19–21] has been gaining popularity. In this case, changes in the distribution of surface sites would be responsible for variability of the product spectrum. Experimental reports of platinum[13, 22, 23], rhodium[24, 25], and gold[25, 26] surfaces undergoing massive restructuring at sufficiently cathodic potentials through a process called cathodic corrosion provide credibility to this theory. Such restructuring during CC has been hypothesized to result from cathodic dissolution mediated by the formation of (ternary) metal hydrides.[24] Given that CO2RR and carbon monoxide reduction (CORR) usually take place under conditions at which cathodic corrosion may occur (i.e., strongly negative potential, high local alkalinity), CC could be a relevant deactivation mechanism for copper electrodes.

In this work, we investigate the (in-)stability of various different copper facets under strongly cathodically corrosive conditions by investigating the evolution in cyclic voltammetry after cathodization in concentrated alkali electrolyte to determine if CC can explain the reported morphology changes of copper under cathodic (CO2RR) conditions. We compare those results to scanning electron microscopy (SEM) experiments conducted on a nanostructured surface prior to- and after running CO2RR to provide relevance to the CO2RR community. Importantly, all experiments were carried out such that accidental surface oxidation was minimized. Both cyclic voltammetry and SEM evidences reported herein indicate that copper is actually stable under purely reducing conditions, and we show that morphological changes as reported in literature are likely related to accidental oxidation/reduction cycles, as opposed to being the result of cathodic corrosion during CO2RR conditions.

5.2. Experimental

5.2.1. Chemicals and electrochemistry

Single-compartment electrochemical cells were made out of fluorinated ethylene propylene bottles (FEP) with appropriately sized machined inlets and outlets for

the working electrode (WE), counter electrode (CE) (Pt, $99.99+$ %), reference electrode (RE, Gaskatel Hydroflex) and ETFE gas tubes. All electrochemical experiments were conducted in such cells. All potentials in this work are reported versus the reversible hydrogen electrode (RHE) unless otherwise specified. Because of reference accuracy limits in the hydroxide environment in combination with high flowrates of argon, the CVs were found to be accurate to within ± 3 mV, which was manually corrected for post-measurement. A standalone annealing compartment made from borosilicate glass and quartz, described elsewhere[27] was mounted on top of the electrochemical cell to enable the annealing of copper crystals in oxygen-free conditions. Argon (Linde, 5.0) was passed through the electrolyte to remove any gases and switched to blanket the solution during electrochemical measurements, unless otherwise specified. In the instances where experiments are conducted in a differing electrolyte (e.g., 10 M NaOH, bicarbonate solution) than the blank electrolyte (0.1 M NaOH), the working cell was switched by unmounting the standalone annealing compartment (with the electrode located inside of it, protected against oxidation by isolating the compartment by closing a key and purging with hydrogen), removing the previous cell and mounting a new cell. After switching the working cell, the electrolyte of the newly-connected cell was purged for ca. 5 $minutes$ to remove any oxygen that was introduced by having to open the cell prior to mounting the annealing compartment on top.

Electrolyte solutions were prepared by dissolving appropriate amounts of chemicals used as received in Milli-Q water (Millipore; resistivity ≥ 18.2 $M\Omega \cdot cm$). Blank voltammograms were conducted in 0.1 M NaOH (99.99%, trace metals basis, Sigma Aldrich), cathodic corrosion experiments were conducted in 10 M NaOH (30.4%, Suprapur, Supelco), CO2RR experiments were conducted in 0.5 M KHCO$_3$ (99.95%, trace metals basis, Sigma Aldrich) purged with CO$_2$ (Linde, 4.7) for at least half an hour. Glassware, plasticware and other relevant parts were oxidatively cleaned in acidic (0.5 M H$_2$SO$_4$, 96%, ACS reagent, Honeywell) permanganate (1 gL^{-1} KMnO$_4$, 99%, ACS reagent, Sigma Aldrich) overnight. Before starting experiments, the permanganate solution was poured out and leftover traces of the solution removed via rinsing with Milli-Q water and washing in a dilute sulfuric acid/peroxide (H$_2$O$_2$, 35%, Ph. Nord, Merck) mix. After washing, residues of the acid washing process were removed by boiling in Milli-Q water for five times.

Platinum CEs were stored in concentrated piranha solution ($3 : 1$ v/v H$_2$SO$_4$: H$_2$O$_2$) after disassembly of the electrochemical cell to prevent copper contamination/alloying. Prior to use, Pt electrodes were rinsed with Milli-Q water and flame annealed with a butane torch. Copper electrodes were cleaned via induction annealing under reducing atmosphere, with the full details described elsewhere.[27] Disk-type electrodes were measured in hanging meniscus configuration, whereas spherical bead-type electrodes were inserted into the electrolyte in their entirety up until where the bead connected to the wire. Cut disk-type electrode CVs were normalized to the geometric surface area, and spherical bead-type Cu(poly) electrodes were normalized to their OH-adsorption charge (determined between -0.25 $V <$ $E < +0.44$ V) using 128.1 $\mu C \cdot cm^{-2}$.[27] Exact crystal pre-treatment and measurement methodologies, including information on CV peak assignments, are described

in a separate work.[27]

5.2.2. Spherical single crystal growth

Spherical single crystals used as is, or as the substrate for the anisotropically roughened electrodes used during identical location SEM investigations, were prepared via the methodology described by Arulmozhi and Jerkiewizc[28], albeit with an alternate nozzle-type that allowed for a central hydrogen-oxygen flame surrounded by an inert argon column. A brief summary of the growth process is as follows.

a. A copper bead was grown from high purity Cu wire (99.9999%, metals basis, Puratronic) via induction annealing in an oxygen-free environment

b. Impurities that migrated from the bulk to the surface were removed by dissolution in concentrated HNO_3 (65%, Ph. Eur., Boom), after which the bead was thoroughly rinsed with Milli-Q water.

c. The bead was briefly remolten (but not grown larger) and allowed to solidify again as per step a), and additional impurities that migrated to the surface were removed as per step b). Re-melting and subsequent surface dissolution/cleaning steps were repeated ca. $5\ times$.

d. The high purity bead electrode was then mounted a few millimeter above the nozzle in a duplicate of the crystal-growing setup as described in [28]. The nozzle, however, was replaced by a different type that allowed for a central flame surrounded by an outer flame, but instead of supplying fuel for an outer flame, argon was fed – resulting in a central flame surrounded by a 'protective' argon blanket.

e. A flame comprised of hydrogen and oxygen in a ratio that was just barely hot enough for melting copper (for our setup, $500 : 57\ sccm$ H_2 : Ar) was used in conjunction with an argon blanket ($800\ sccm$) and positioned such that ca. 75% of the copper bead was molten.

f. After a brief stabilization period (ca. $5 - 15\ minutes$) the nozzle was then gradually decreased in height via a computer-controlled micro-actuator located at the base of the micro-torch, allowing for the copper melt to slowly solidify.

g. After the entirety of the (now single crystalline) bead had solidified, the flowrate of the Ar blanket was increased to $1500\ sccm$ in one step and the oxygen content of the flame lowered in ca. 20% increments until reaching zero over a period of ca. $30\ seconds$.

h. Subsequently, the hydrogen flowrate was gradually reduced in ca. 1% increments, whilst the argon flowrate was increased in 1% increments until the hydrogen flame extinguished from a lack of oxygen (coming from the ambient air, diffusing through the argon blanket). Decreasing the hydrogen flowrate to ca. $100\ sccm$ resulted in the flame being unable to persist for our system.

i. Then, the crystal was allowed to cool to room temperature in the reducing atmosphere of ca. $2000 : 100$ Ar : H_2 for ca. $10 - 15\ min$.

5.2.3. Anisotropic roughening

Creation of anisotropic roughness with μm-scale morphology was obtained in a controlled manner by using a strategy reported by Sloan *et al.*[29] Briefly, we cycled the electrode in CO_2-purged bicarbonate ($0.1\ M$) electrolyte with $4\ mM$ KCl from $-0.75\ V$ to $+0.70\ V$, and back down to $-1.5\ V$ at a scan rate $\nu = 5\ mV \cdot s^{-1}$. Then, $-1.5\ V$ was applied for another ca. $5\ minutes$. The exact potentials and number of cycles (i.e., 1) were adjusted from the original work so as to prevent losing anisotropic effects due to over-oxidation, with a period at highly reducing potentials included to guarantee full reduction of the surface.

5.2.4. Interfacing between electrochemistry and SEM

In case of post-electrochemical treatment investigation of the surface via SEM, the following methodology was employed to limit surface oxidation of the crystals. It is very important to make sure the surface is completely dry prior to exposure to air where it cannot be avoided, so as to decrease the rate at which the surface oxidizes.

a. Finish the electrochemical experiment

b. Break electrical contact and increase hydrogen flow to several $L \cdot min^{-1}$ (adjusted manually, exact flowrate unknown).

c. Move electrode up, to where the annealing compartment of the setup is connected to the electrochemical cell (see [27])

d. Move the entirety of the annealing compartment containing the electrode up, breaking the link with the electrochemical cell. This action creates an opening where the annealing compartment is now exposed to ambient conditions but as this location is the path of least resistance for the hydrogen to flow, the crystal is still under reducing conditions provided the hydrogen flow is sufficiently high.

e. Move the crystal slightly down, so that it is sticking out of the annealing compartment a few millimeters.

f. Thoroughly rinse the crystal with Milli-Q water (ca. $30\ seconds$), being careful to only wet the crystal surface and not to allow water to flow up to (and down from) where the connecting wire of the crystal is attached to the electrode holder.

g. Move the crystal up through the keyhole to inside of the annealing compartment and close the key, creating a water-locked isolated environment.

h. Decrease hydrogen flow to several hundred sccm (exact flowrates unknown), making sure that the gas is exiting through the water lock.

i. Dry the electrode in the annealing compartment under active hydrogen flow for ca. $15 - 30 \; minutes$.

j. Stop hydrogen flow and take the electrode out of the setup. Fixate the electrode in a SEM holder, and place the holder in a desiccator or other type of vessel that can be depressurized. Attach the desiccator with crystal inside to a pump and depressurize to ca. $1 - 5 \; mbar$, and close off the desiccator. Total exposure of the (dry) crystal to ($1 \; atm$ of) air during this period is ca. $45 - 60 \; seconds$.

k. Move the desiccator to where the SEM is located and place the crystal in the SEM chamber, close it off and start pumping down. During this period, the (dry) crystal is exposed to ($1 \; atm$ of) air for another ca. $30 - 45 \; seconds$.

5.2.5. Instruments and software

All electrochemical experiments were conducted with a VSP-300 potentiostat from BioLogic, controlled with their proprietary software EC-Lab. Where applicable, gas flowrates were controlled via mass flow controllers from Brooks (SLA5850) via their proprietary software. Data editing and plotting was done using the software Igor. The SEM was operated under high vacuum ($\leq 8 \cdot 10^{-6} \; mbar$), with micrographs collected with beam settings of $15 \; kV$ and $0.40 \; nA$ utilizing an Everhart-Thornley detector. SEM images have been subjected to post-acquisition editing in photoshop, possibly having been i) rotated, ii) cropped and/or iii) having had their contrast and brightness adjusted.

5.3. Results and discussion

5.3.1. Cathodic surface stability from CV studies

To study if copper undergoes cathodic restructuring, experiments were conducted under literature-reported conditions that maximize the chance of cathodically-induced morphological changes occurring: high alkalinity, high cation concentration, and strongly negative potentials.[13, 22–25] Stability studies were conducted in $10 \; M$ NaOH at the maximum cathodic potential that could be applied by our potentiostat with 85% iR correction turned on, being $-1.75 \; V$ vs. RHE. Furthermore, our experimental setup was carefully constructed such that it allowed us to fully prevent surface oxidation unless deliberately induced via electrochemical means. Experiments were performed in the absence and presence of surface oxides to determine the effect of oxidation on the apparent cathodic stability of copper. Where applicable, pre-oxidation was done at $+0.50 \; V$ considering that this potential is only a few millivolts positive of the open circuit potential (OCV) for copper in our electrochemical environment. Corrosion times (cathodic and anodic) were set at $1 \; minute$, so as to minimize any possible influences of contaminants and to prevent electrolyte heating from influencing the results. Experiments for longer time periods, at different cathodic potentials, and under different electrolyte conditions are described in the second half of this work.
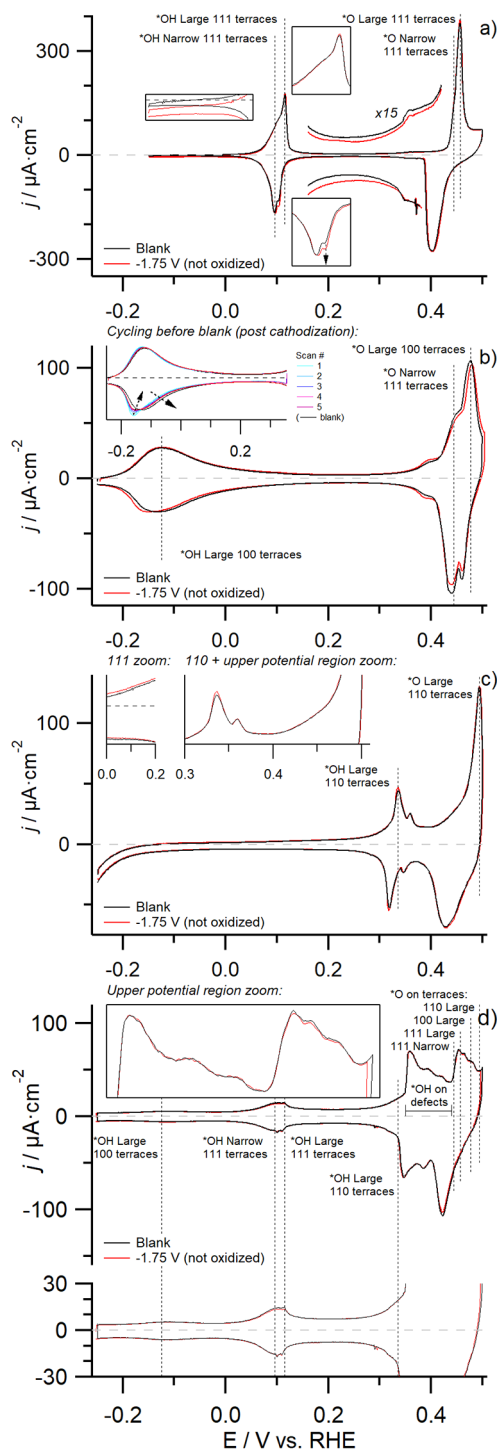
Characterization CVs ($0.1 \; M$ NaOH) obtained after cathodization in both the

absence (Figure 5.1) and presence (Figure 5.2) of surface oxides are compared to their initial characterization CVs (blank CVs), to study the cathodic stability of metallic copper and how the presence of a native oxide layer influences this stability. Reference inaccuracies resulted in upper potential limits varying ca. $3\ mV$, which actually influences the results slightly considering the upper potential we employ in this work is right at the onset of bulk copper oxidation. Therefore, depending on the exact situation, we may forego discussing changes in the negative going scan, especially if those differences are located close to the upper potential limit of the CV. Considering that all surfaces exhibit comparable behavior under purely cathodic conditions, we shall discuss the results of cathodic-only experiments ($1\ min$ at $-1.75\ V$ in $10\ M$ NaOH) first, depicted in Figure 5.1, where the initial blank CV for the various surfaces is shown in black and the CV obtained after cathodization in red.

The CV of a Cu(111) surface after one minute of cathodization is depicted in Figure 5.1a. Various insets depicting magnifications of the double layer regions and main OH-adsorption feature are included for clarity. We find that the CVs before (black) and after (red) cathodization are strikingly similar if we ignore a minor cathodic offset of the CV between $-0.15\ V < E < +0.30\ V$ as that can be attributed to trace amounts of oxygen in the electrolyte (not actually influencing the CV shape, only resulting in a cathodic offset). Actually, only one difference is observed, namely that the twinned cathodic OH-adsorption feature for the {111}-terraces at $+0.1\ V$ shows a minute increase in charge for the more positively located peak (denoted by an arrow in the inset), though this effect is virtually absent in the anodic feature. In our previous work[27] we hypothesize that the split nature of the {111}-specific OH-adsorption feature is a function of terrace length, with a broader adsorption feature located at more negative potentials being related to relatively smaller terraces and a sharp feature located at slightly more positive potentials being related to (very) large terraces. If the narrower {111}-specific feature indeed relates to larger terraces, as we propose, then the CV we obtain after applying cathodic potentials denotes an increase in the number of such larger terraces. This minor increase in surface crystallinity is very likely a result of the fact that we reanneal the surface prior to conducting cathodization experiments, having resulted in a marginally smoother surface. From the (absence of) observed differences, we conclude that the copper {111} face is stable against purely cathodic conditions.

The same experiment was also conducted on Cu(100) and is depicted in Figure 5.1b, where black denotes the blank and red the CV after cathodization. An inset depicting the 'pre-cycling' phase is included as we found that {100} terraces reconstruct during this period if the surface had been treated cathodically (but not after induction annealing, i.e., before the blank). During this phase (inset Figure 5.1b) we find that the {100}-specific OH-adsorption feature at $-0.125\ V$ is initially fairly asymmetrical but becomes increasingly symmetrical with successive cycling (e.g., going from the blue to the purple CV) although the initial level of symmetry is never regained, even if the number of cycles during this period is increased (not depicted).

These observations for pre-cycling carry over to the full-window post-cathodization characterization CV (red) where it can be seen that the cathodic peak at $-0.125\ V$ is

Figure 5.1: The effect of applying a cathodization period on the characterization CV ($0.1\ M$ NaOH, $v = 50\ mV \cdot s^{-1}$) of copper surfaces of various orientations devoid of initial surface oxides. Panels a-d) represent the voltammograms obtained prior to- (black) and after (red) a cathodization period ($1\ min$ at $-1.75\ V$, 85% iR corrected) in $10\ M$ NaOH for an a) Cu(111), b) Cu(100), c) Cu(110) and d) Cu(poly) surface.

shifted to slightly more negative potentials thus resulting in decreased reversibility of the overall feature. Additionally, it can be seen that the reversible defect-related peak located at $+0.38\ V$ exhibits increased charge, signifying an increase in defect sites. As a third difference we find that the {100}-specific O-adsorption feature at $+0.477\ V$ shifts to slightly more positive potentials whilst slightly decreasing in maximum intensity, resulting in decreased current in the region $+0.42\ V < E < +0.48\ V$ and increased current for $E > +0.48\ V$. We believe that the positive shifting of this feature signifies a decrease in average {100} terrace width, which matches with the observed increase in defect density. These minor CV changes for Cu(100) could possibly be the result of (partially) irreversible potential-induced surface reconstruction at negative potentials. Such cathodic reconstruction of the {100} face has been reported by Matsushima *et al.*[15] who show via in-situ scanning tunneling microscopy that, under sufficiently negative potentials in $0.1\ M$ HClO$_4$, a fraction of the atoms at the Cu(100) surface form rows that are slightly elevated with respect to the rest of the surface. If this so-called hydrogen-induced reconstruction[15] is not fully reversible, it can reasonably explain the minor differences observed in our cyclic voltammetry, considering that the CV changes we discuss represent an overall decrease in surface crystallinity. Although we find that the {100} face is not perfectly stable under cathodic-only conditions, the changes are still relatively minor.

CVs of a Cu(110) surface before (black) and after (red) cathodic polarization are shown in Figure 5.1c. Post-cathodization voltammetric behavior similar to that of a Cu(111) surface is observed, i.e., mostly an absence of change. One minute difference can be observed by looking at the amount of anodic and cathodic charge associated with the {110}-feature located at ca. $+0.33\ V$, which is found to increase slightly – signifying a small increase in surface crystallinity. This minor increase in crystallinity is not so strange, considering that the methodology we employ for generating a stable {110} surface involves evolving large amounts of hydrogen at very negative potentials, similar to the cathodic treatment we use for the results depicted in this figure. No other deviations are observed, and thus we arrive at the same conclusion as for the other two faces: the {110} facet is stable under cathodically corrosive conditions.

Finally, we depict CVs of Cu(poly) in Figure 5.1d. By their nature, polycrystalline surfaces contain a higher fraction of undercoordinated sites such as step and kink defects. This is evident from the presence (and intensity) of a number of additional features between $+0.35\ V < E < +0.44\ V$. Due to the different sizes of crystallites present on the surface, it will also contain a wider gamut of terrace sizes. Hence, experiments on a Cu(poly) electrode can provide additional insights into the cathodic stability of more reactive, and therefore generally assumed more catalytically active, sites. Investigation of the CV after the experiment (red) shows very little change compared to the initially obtained blank CV (black). Scrutinizing closely, small deviations can be seen around $+0.1\ V$, and between $0.44\ V < E < 0.48\ V$, which relate to changes in {111} terrace sites and {100} terrace sites, respectively. The small decrease in OH-adsorption on {111} terraces ($+0.1\ V$) can actually be attributed to the fact that we sweep the potential to $E < -0.15\ V$, which has been

reported in literature to result in suppression of the associated anodic feature.[30] Taking into consideration that the negative potential limit was slightly more negative after cathodization due to reference inaccuracies, the minor difference at ca. $+0.1\ V$ is likely caused by the slight variation in lower CV boundaries. This leaves a diminutive difference in O-adsorption related to {100}-terrace sites ($+0.477\ V$), which is in line with what we discussed previously for Cu(100), namely that likely some irreversibility is associated with lifting the hydrogen-induced reconstruction of this face. Therefore, we conclude that also a defect-rich Cu(poly) surface is stable under strongly cathodic conditions, with mostly {100} terrace-sites being mildly impacted.

A second set of experiments was conducted based on the notion that it is challenging to guarantee oxygen-free, non-oxidizing conditions when utilizing default literature procedures, surface preparation methodologies and prevalent experimental setups. To this end, a pre-oxidation step ($1\ min$ at $+0.50\ V$, close to the OCV of Cu in our system) prior to cathodization was purposely included in a set of control experiments, to compare the cathodic stability of copper in the presence of a native oxide film with our results in the absence of surface oxides. Pre-oxidation investigations at more positive potentials were also investigated for Cu(110) and Cu(poly) surfaces, considering that they exhibited very mild changes at $+0.50\ V$. The results are depicted in Figure 5.2, where initially obtained blank CVs (black) for the various surfaces under investigation are compared to the characterization CV as obtained after pre-oxidation cathodization experiments in $10\ M$ NaOH (red) where the surface was first pre-oxidized ($1\ min$ at $+0.50\ V$), prior to stepping the potential to cathodic potentials ($1\ min$ at $-1.75\ V$).

The effect of adding a pre-oxidation step on the cathodic stability of a Cu(111) surface can be determined by comparing the CVs in Figure 5.1a (absence of oxidation) with those in Figure 5.2a (presence of oxidation). To determine this effect, we first have to analyze what CV changes occur for a surface that has been pre-oxidized before cathodization by comparing the initial CV (black) to the CV obtained after the experiment (red) in Figure 5.2a. A first difference can be seen at the negative potential limit of the CV ($E < 0\ V$), where excess cathodic charge is observed after pre-oxidation plus cathodization treatment. Considering that this current is not related to the ORR (its onset being at too negative a potential for that – e.g., compare it to the more positive onset for ORR-related current in the red trace in Figure 5.1a), we tentatively attribute it to the hydrogen evolution reaction (HER) instead. Second, we see that the oxidative {111}-terrace peak at $+0.1\ V$ shows reduced peak intensity which looks to be associated with increased charge at slightly more positive potentials (ca. $+0.105\ V$). Additionally, a new anodic feature is observed to develop at ca. $+0.235\ V$. Furthermore, we find that the reversible defect-related feature around $+0.35\ V$ grows in intensity. None of these effects were observed in the absence of a pre-oxidation treatment. Lastly, we observe increased charge of the more positive peak of the cathodic feature at $+0.1\ V$. This is in agreement with what we observe in the absence of surface oxidation, though in that instance the anodic charge did not decrease.

The increased HER activity of a pre-oxidized and subsequently cathodized Cu(111)
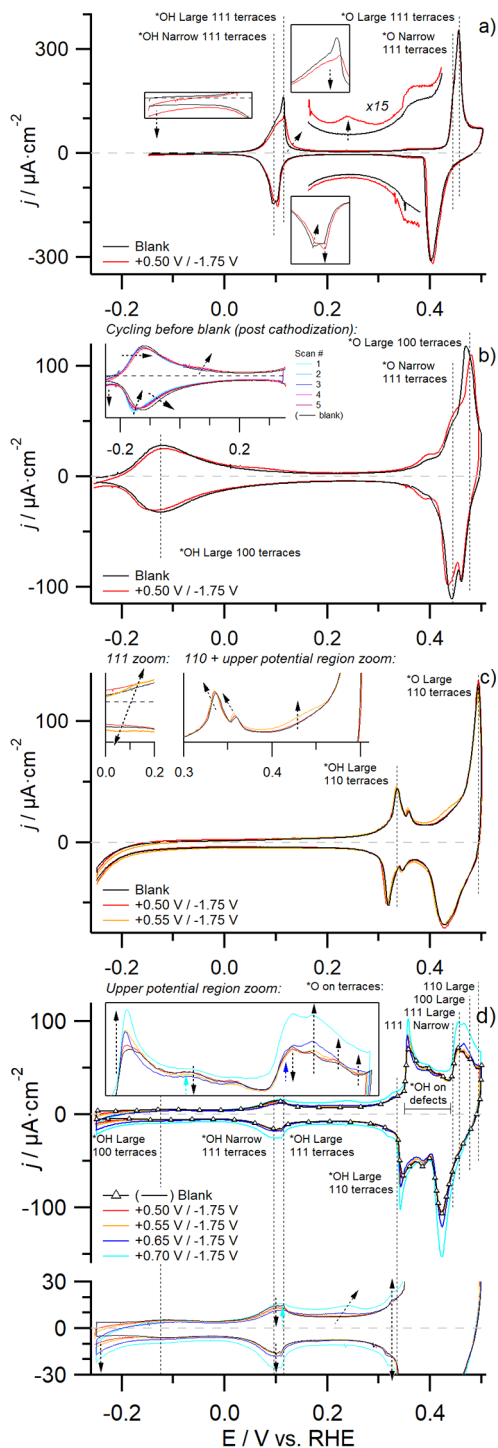
Figure 5.2: The effect of applying a pre-oxidation period followed by a cathodization period on the characterization CV ($0.1\ M$ NaOH, $v = 50\ mV \cdot s^{-1}$) of copper surfaces of various orientations devoid of initial surface oxides. Panels a-d) represent the voltammograms obtained prior to- (black) and after (red) a pre-oxidation period ($1\ min$ at $+0.50\ V$, 85% iR corrected) followed by a cathodization period ($1\ min$ at $-1.75V$, 85% iR corrected) in $10\ M$ NaOH for an a) Cu(111), b) Cu(100), c) Cu(110) and d) Cu(poly) surface. More positive oxidation potentials were also investigated for the Cu(110) ($+0.55\ V$ only) and Cu(poly) electrodes, which are depicted in orange, blue and cyan for $1\ min$ of oxidation at $+0.55\ V$, $+0.65\ V$ and $+0.70\ V$, respectively.

surface, combined with the appearance of a new, irreversible anodic feature at $+0.235\ V$ and an increase in charge of the feature at $+0.35\ V$ all indicate additional defect sites. This is corroborated by the fact that we observe the peak intensity of the {111}-specific OH-adsorption feature at $+0.1\ V$ going down, whilst simultaneously seeing an increase in charge in the region located at slightly more positive potentials. We hypothesize this represents a decrease in average terrace width, considering that a literature-reported Cu(211) CV (denoting a 3(111)x(100) surface) exhibits a similar broad charge contribution at potentials positive of $+0.1\ V$.[31] We realize that it is peculiar that the increase in oxidative charge at $E > +0.1\ V$ that we attribute to small-width {111} terraces is not matched by a similar increase in cathodic charge in the negative-going scan, as is the fact that the suppression of charge of the anodic feature at $+0.1\ V$ is (mostly) absent for the cathodic feature. A possible explanation for this would revolve around the irreversible nature of O-adsorption on {111} terrace sites as evidenced by the asymmetry of the feature at $+0.457\ V$. Possibly, shorter (i.e., defect rich) terraces are influenced more strongly by oxygen desorption resulting in reconstruction of these sites in the reverse scan direction. Overall, by comparing the respective CV changes of Cu(111) when it has been cathodized either in the absence or in the presence of a pre-oxidation step, it is clear that surface oxides negatively impact the stability of {111} terrace sites under cathodic conditions – and thus, by association, are likely to result in changing their morphology.

Next, we study the effect of the presence of surface oxides on the cathodic stability of Cu(100). The characterization CVs of this face after cathodization in the absence and presence of a pre-oxidation period are shown in Figures 5.1b and 5.2b, respectively. Once again, an inset with the pre-cycling CVs is provided in Figure 5.2b with the initial blank CV and CV after pre-oxidation plus cathodization treatment depicted in black and red in the submain figure, respectively. In line with our initial discussion for this facet, already during the pre-cycling phase surface reconstruction is apparent. Specifically, for the pre-oxidized and subsequently cathodized electrode, we observe the following behavior during this initial phase (inset Figure 5.2b). Firstly, similar to a non-oxidized surface, we observe that the feature at $-0.125\ V$ starts off asymmetrically, but becomes more symmetrical with successive cycling (going from the blue to the purple line), with the cathodic peak shifting to more positive potentials. Again, the initial symmetry of the feature is not fully recovered. In contrast with cathodic-only treatment, a number of additional changes are observed during this pre-cycling period in the case of pre-oxidation. Aside from the cathodic peak at ca. $-0.125\ V$ shifting, the oxidative peak is actually observed to shift slightly as well. Furthermore, the total charge of the {100} adsorption feature is observed to diminish. Additionally, an anodic shoulder grows in at ca. $+0.075\ V$; relatively close to where one would expect {111} terraces to contribute charge (+0.1 V) although no associated cathodic peak is observed. Finally, HER activity at negative potentials ($E < -0.2\ V$) increases with successive cycling.

All of these effects carry over when we compare the full-window characterization CV (red) with the initial blank CV (black): excess cathodic charge is observed for

$E < 0.2\ V$, the {100} adsorption feature at $-0.125\ V$ is overall less symmetrical and exhibits suppressed charge, and an oxidative 'bump' near $+0.075\ V$ is visible. The suppression of the overall charge of the OH-adsorption feature was not observed in the case of a cathodic-only treated Cu(100) crystal (Figure 5.1b), nor was the formation of a feature near $+0.075\ V$. Additional observed changes for the full-window CV are that more crystal defects are present as indicated by increases in charge for both the step-related feature at ca. $+0.38\ V$ and the {111}-terraces related shoulder near $+0.445\ V$. Increases in the number of step sites was also observed without surface oxidation, but increases in {111} terrace sites were not. Finally, the {100} O-adsorption feature ($+0.477\ V$) is observed to both decrease in intensity and shift towards more positive potentials. This agrees with what we observed in the absence of surface oxidation, but is more pronounced after pre-oxidation.

From the combination of increased HER activity, the appearance of a new feature at $+0.075\ V$, an increase in the charge of the reversible defects-related feature near $+0.38\ V$ and the growth of the shoulder at ca. $+0.445\ V$ (likely related to the formation of small {111} terrace sites[27]) it is clear that additional defects are being formed in the surface. Similar to the previous discussion, this is corroborated by the loss of symmetry and decrease in intensity of the {100}-related feature near $-0.125\ V$, for which we know from a literature-reported Cu(911) CV (denoting a 5(100)x(111) surface)[32] that the OH-feature for shorter {100} terraces is located at more negative potentials. We also observe the {100}-specific O-adsorption feature at $+0.475\ V$ to shift to more positive potentials (making it overall less reversible) and decrease in intensity, both of which can be similarly interpreted as the behavior observed for the main OH-adsorption feature at $-0.125\ V$: a decrease in surface crystallinity. Considering that these changes are more numerous and more pronounced than for the cathodic-only experiment, it is clear that the presence of surface oxides results in decreased stability of {100} terrace sites and thus increases the likelihood of morphological evolution taking place.

Next, we investigate the effect of pre-oxidation on the cathodic stability of Cu(110), with Figures 5.1c and 5.2c showing the CVs obtained before (black) after (red) cathodization in the absence and presence of a pre-oxidation period at $+0.50\ V$, respectively. Due to the very small differences observed for a pre-oxidation potential of $+0.50\ V$ (red), an additional experiment was conducted at $+0.55\ V$ (orange). When carefully scrutinized, both samples exhibit the same CV changes, but we will discuss the latter since there the changes are more prominent. When comparing the orange trace to the initial blank (black), we observe the following. Firstly, we find increased HER activity at potentials $E < -0.1\ V$. Secondly, a reversible feature near $+0.1\ V$ develops, being a clear indication of the formation of {111}-terrace sites. Thirdly, the amount of charge of the {110}-specific OH-adsorption feature at $+0.33\ V$ is found to increase slightly, similar to the non-oxidized sample. However, we see an additional change for this feature, being a shift to slightly more negative potentials. Further differences are observed in the form of increased charge for the symmetrical, defect-related feature at ca. $+0.35\ V$, which is additionally observed to also shift to slightly more negative potentials. Finally, we observe increased

charge in the potential range $0.375\ V < E < 0.46\ V$, where both defect sites and {111} terraces exhibit adsorption behavior.

Compared to Cu(111) and Cu(100), Cu(110) exhibits less prominent changes when pre-oxidized, necessitating an increase in the oxidation potential from $+0.50\ V$ to $+0.55\ V$ to observe changes of similar magnitude as seen for pre-oxidized {111} and {100} surfaces. However, the overall conclusion after comparison of CV behavior in the absence and presence of surface oxides is in agreement with previously discussed faces: oxidation negatively impacts the cathodic stability of Cu(110).

Lastly, we also investigated the behavior of a Cu(poly) electrode, depicted in Figures 5.1d and 5.2d, for cathodization in the absence and presence of pre-oxidation, respectively. Considering such a surface is easily remade if irreversible surface damage is observed, a wider range of pre-oxidation potentials was investigated. Specifically, depicted in Figure 5.2d in red, orange, blue and cyan are, respectively: $+0.50\ V, +0.55\ V, +0.65\ V$ and $+0.70\ V$ (with $+0.60\ V$ falling in-between $+0.55\ V$ and $+0.65\ V$, not depicted). At the bottom of the figure a narrower current range is provided, giving a clearer view of the changes in the region between $-0.25\ V < E < +0.35\ V$. Considering that the voltammetric behavior we observe is (almost) identical up to a pre-oxidation potential of $+0.65\ V$ (blue), we shall discuss that particular datapoint.

Similar to the principal faces, we find that a pre-oxidized and subsequently cathodized polycrystalline copper surface exhibits increased HER activity at $E < -0.1\ V$. This increase is likely related to an increase in defect density, although it may also signify an increase in the number of {110} terrace sites or a combination of the two. Due to increased HER current, it becomes difficult to ascertain if the {100} OH-adsorption feature at $-0.125\ V$ is changing or not because of convolution effects. However, clear changes are observed for OH-adsorption on {111} terraces, with the anodic peak at $+0.1\ V$ exhibiting decreased current density, although this is not reflected in a decrease of the associated cathodic peak (which stays equal for $+0.50\ V$ and $+0.55\ V$, and conversely increases in the case of $+0.65\ V$). Concomitantly with the decrease of the anodic peak at $+0.1\ V$, an increase in anodic (but not cathodic) charge is observed in the potential window that directly follows, between ca. $+0.1\ V < E < +0.3\ V$. Similar behavior was observed for Cu(111), where we hypothesized it represents a decrease in average terrace width, whilst the mismatch between anodic and cathodic charge trends is possibly related to the irreversibility of oxygen adsorption resulting in reconstruction of the (defect-rich) terraces.

Increased charge at $+0.33\ V$ is also observed, signifying that additional {110} terraces are present. Then, between $+0.35\ V < E < +0.44\ V$ (where OH adsorbs on defects) we find increased charge centered around $+0.356\ V$, whilst the rest of the window remains equal ($+0.42\ V < E < +0.44\ V$) or decreases in charge ($+0.37\ V < E < +0.42\ V$). Taken together, this represents anisotropic surface restructuring with some types of defects increasing and other types of defect sites decreasing in abundance. In the upper potential region of the CV (*O region, $E \geq +0.44\ V$) we see the following. Between $+0.44\ V < E < +0.458\ V$ (O-adsorption on {111} terraces) a small decrease in charge is observed for pre-oxidation at $+0.50\ V$

and $+0.55\ V$. However, from $+0.65\ V$ on, the charge starts increasing. The initial decrease can readily be explained by anisotropic effects, with the (originally fully reduced) {111} terrace sites being lost as they interconvert into other types of sites when oxidized and subsequently reduced. However, as a reversal in behavior is observed with peak charge increasing for $E \geq\ +0.65\ V$, a secondary process operating in parallel with the first mechanism must exist via which new terrace sites form. Likely, this additional pathway has to do with the creation of pits in the surface through dissolution and/or the formation of deposits through electroplating of (in-operando generated) Cu ions. The last section of the CV ($E > +0.458\ V$) exhibits monotonous increase in charge as a function of pre-oxidation potential, representing increases in the amount of both {100} and {110} terrace sites.

Clearly, oxidation and subsequent reduction of copper is anisotropic; with some types of defect and terrace sites decreasing and other types of defect and terrace sites increasing, representing their interconversion. However, as the pre-oxidation potential is increased, the initial stages of surface roughening can be observed as evidenced by the reversal of the behavior of O-adsorption on {111} terraces (decreasing to increasing as oxidation potential is increased). This roughening of the surface becomes more pronounced as the pre-oxidation potential is increased to $+0.70\ V$ (Figure 5.2d, cyan), with the entirety of the CV exhibiting increased current density. This represents an increase in the number of every type of site, which can only be valid if overall surface area is increasing (i.e., roughening of the surface). Such roughening (i.e., changing morphology) can be explained if we either start forming pits in the surface via dissolution[11] and/or start forming particles atop the surface (e.g., due to redeposition phenomena). Roughening of copper in the absence and presence of a pre-oxidation period is further investigated in the following section, where we use SEM to investigate various locations on a spherical single crystal.

5.3.2. Microscopy study of surface roughening in the absence and presence of copper oxides

So far, we employed CV studies to investigate the (absence of) change in surface morphology of various copper substrates under purely cathodic conditions. Supporting evidence for the voltammetric behavior observed in the presence and absence of a pre-oxidation period is provided in the form of SEM imaging. For this study, a spherical single crystal was used as a model catalyst considering that it allows for comparison of substrates of (initially) comparable crystallographic orientation. The exact procedure was as follows. Firstly, the single crystal was pre-oxidized in $10\ M$ NaOH at $+0.70\ V$ for $1\ minute$ prior to being cathodized at $-1.75\ V$ for $1\ minute$ (equal electrochemical treatment to the cyan trace in Figure 5.2d), whereafter it was moved to the SEM for investigating the morphology. Exact imaging locations were documented to allow for re-visiting them later on. Then, the crystal was (mostly) recovered to its initial state by flame annealing it in a H_2/O_2 flame for ca. $30\ min$ near the melting point of copper (CV reproducibility depicted in Figure D.1). Next, a cathodic-only experiment was conducted by applying $-1.75\ V$ for $5\ minutes$ in $10\ M$ NaOH, where the experiment duration was intentionally

increased five-fold (from $1\ min$ to $5\ min$) as preliminary results indicated no discernible roughening after $1\ min$ of cathodization (not depicted). After rinsing and drying, the crystal was then moved to the SEM and manually positioned to match as best as possible its orientation during the previous experiment based on the visible (static) locations of the {100} and {111} planes. Then, previously investigated locations were revisited and imaged again. As the orientation of the crystal in the SEM chamber was manually adjusted between experiments, the incidence angle of the electron beam with respect to the surface normal is not exactly equal between corresponding sets of images nor is it necessarily always exactly perpendicular to the surface. Furthermore, slight mismatches of this angle between images are exacerbated by the fact that the surface has a curvature in all directions, considering that the study was conducted on a spherical single crystal. The micrographs obtained for both conditions are depicted in Figure 5.3 in the form of numbered pairs (e.g., 1 and 1), for which we estimate that the respective sets of images between the different experiments were located within $< 100\ \mu m$ of each other on the surface (yielding comparable initial substrates).

By imaging various spots along the vertices of a stereographic triangle, we were able to investigate a wide variety of substrates and obtain results that should be representative of the overall behavior of a polycrystalline surface. And because we employ a spherical single crystalline surface, we can compare locations on the crystal for different experiments that were initially of the same crystallographic orientation. Hence, we can relate changes in morphology to changes in experimental conditions in an unbiased manner as substrate-directing effects are mitigated (contrary to if similar experiments were to be conducted on polycrystalline surfaces). We compare the final morphology of a surface that was treated purely cathodically ($-1.75\ V, 5\ min$) with that of a surface that was firstly oxidized ($+0.7\ V, 1\ min$) and then treated cathodically ($-1.75\ V, 1\ min$) to determine the influence of surface oxidation on the morphological restructuring of copper.

In Figures 5.3a and 5.3c, we show the overall profile of the crystal after cathodization ($-1.75\ V$) in the presence of pre-oxidation at $+0.70\ V$ and in the absence of pre-oxidation, respectively. In these subfigures, the contrast and brightness of the {111} plane were adjusted independently to enhance its visibility. The original single-crystalline nature of the crystal is clear from Figure 5.3a, considering that the anisotropic oxidation resulted in distinct regions on the surface that repeat as expected of the symmetry of the FCC unit cell (see e.g., here[33] for further information). In Figure 5.3c (in the absence of oxidation) no such distinct regions are observed, but the {100} and {111} basal planes (denoted by the □ and ○ symbols, respectively) could be located, which then allowed for determination of the location of the {110} plane, completing the stereographic triangle. 'Proof' that the main facets as indicated by the symbols are indeed located where we claim is provided in the form of close-ups of those regions given in Figure 5.3g, where the top row was obtained in the presence of pre-oxidation and the bottom row in the absence of pre-oxidation. In Figure 5.3e, a rotated and magnified view of Figure 5.3a is presented, with numbering added to represent the approximate locations where micrographs were obtained.
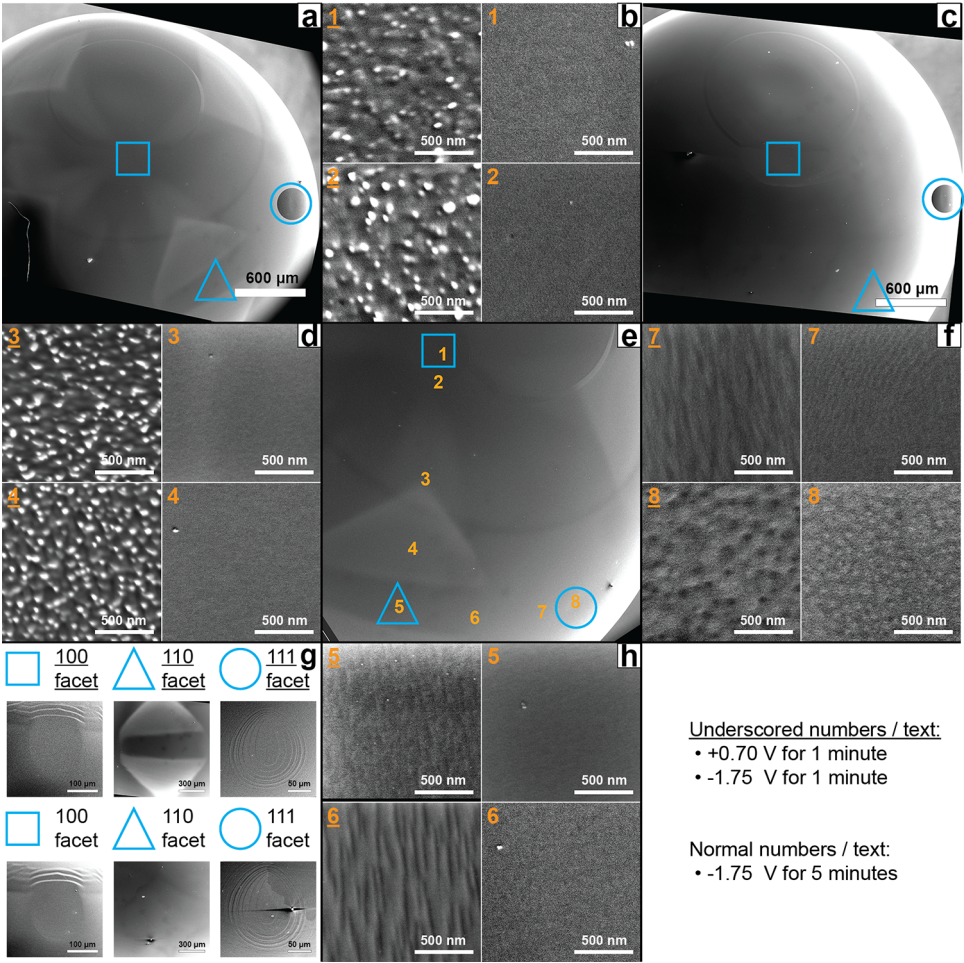
Figure 5.3: Comparison of close-proximity location SEM images for an identical spherical single crystal that was either subjected to a cathodic-only period ($-1.75\ V$ for $5\ min$) or firstly pre-oxidized ($+0.7\ V$ for $1\ min$) before applying a cathodic period ($-1.75\ V$ for $1\ min$) in $10\ M$ NaOH. Overview images for the pre-oxidized and cathodic-only treated crystal are given in panels a) and c), respectively. Close-ups of the basal planes (represented by the following symbols: □ for {100}, △ for {110} and ○ for {111}) are provided in panel g), where only two out of three need to be visible for accurate determination of the location of a stereographic triangle. Approximate imaging locations along the vertices of the stereographic triangle as defined by the three respective basal planes are represented by the numbers in orange in panel e). High-magnification micrographs of the locations matching the numbering of panel e) are depicted in panels b), d), f) and h), with the number matching the location given in the top-left corner where side-by-side sets represent micrographs obtained in matching locations for either cathodic corrosion in the presence of a pre-oxidation step (left-hand side, with underscored numbering) or in the absence of pre-oxidation (right-hand side, with normal numbering).

Having established the crystallinity of the surface and determined the location of one of the stereographic triangles, we now investigate a number of locations along the vertices of the triangle to represent the cathodic stability of copper of various crystallographic orientations in Figures 5.3b, d, f and h. In each of these subfigures, the morphology of two different spots on the surface in the presence of pre-oxidation (left-hand side) are compared to representative locations without oxidation (right-hand side), with numbers in the top-left corner of the respective images matching the locations given in Figure 5.3e. Comparing the surface morphologies in Figures 5.3b, d and h, we find that surface roughening is below the detection limit of the SEM in the case of cathodic-only treatment ($-1.75\ V, 5\ min$), requiring random traces of dust for focusing. However, clear anisotropic roughening is present if a pre-oxidation step ($+0.70\ V, 1\ min$) is included prior to cathodization ($-1.75\ V, 1\ min$). An exception to this is seen in Figure 5.3f, wherein locations close to the {111} face are depicted. In this case, some (albeit less) roughness is also observed in the case of cathodic-only treatment. This actually agrees with small changes in voltammetry (Figure D.1) observed after recovery of the surface via H_2/O_2 annealing, considering that the {111} terrace-related OH-adsorption peak ($+0.1\ V$) exhibited slightly increased charge after flame annealing compared to the CV obtained prior to the pre-oxidation experiment. As such, we are unsure if the roughness we observe from SEM near the {111} face is because of the cathodic treatment, or because the annealing treatment failed to fully recover the surface to its initial state.

The key take-away from this measurement is that a partially oxidized surface results in significant roughening during cathodization, whereas a fully reduced surface yields no observable roughening. Furthermore, the roughening under pre-oxidized conditions is anisotropic, in agreement with CV results (Figure 5.2d). Although we realize that the spatial resolution of the SEM is limited, the results we obtain are in line with what we observe also from voltammetry: high stability of copper with respect to purely cathodic conditions that is negatively impacted by the presence of surface oxides.

5.3.3. (Absence of) time-dependent morphological change

Up to now, the results reported here have been regarding the stability of copper under aggressively cathodic potentials ($-1.75\ V$ vs. RHE) in strongly alkaline media ($10\ M$ NaOH) for relatively brief periods of time ($1\ min$, except for the cathodic-only SEM data reported in Figure 5.3; $5\ min$). We realize that such conditions may not represent the reported morphological instability of copper during CO2RR operation, considering that electrolyte composition and experiment duration differ significantly, implying that possible effects by e.g., (adsorption of) carbonaceous species are not included. To this end, we performed voltammetric studies before and after the following experiments: i) equal conditions as discussed so far ($-1.75\ V$ in $10\ M$ NaOH) but for increased reaction times ($5, 15$ and $60\ min$, Figures 5.4a and 5.4b, respectively) and ii) employing CO2RR-representative conditions ($60\ min$ at $-0.75\ V$ in $0.5\ M$ KHCO$_3$, Figure 5.4c). The upper boundary of $60\ min$ was chosen based on literature-reported chronoamperometry data exhibiting a clear trend of

decreasing CO2RR activity of various copper surfaces on this timescale by multiple authors.[7, 10, 21, 34, 35]

Blank CVs ($0.1\ M$ NaOH) obtained prior to and after extended cathodization periods in either $10\ M$ NaOH or $0.5\ M$ KHCO$_3$ are depicted in Figure 5.4, where close-ups of relevant regions are provided as insets and trends discussed in text denoted by arrows. Figure 5.4a depicts CVs obtained initially (i.e., the blank) and after 5 and $15\ minutes$ of cathodization ($-1.75\ V$) in $10\ M$ NaOH in black, yellow and blue, respectively. Unlike for $1\ min$ of reaction time (Figure 5.1d) under otherwise identical conditions, minor changes in voltammetry can be observed in this instance. Specifically; a small increase in HER activity (denoted by increased cathodic current for $E < -0.1\ V$), suppression of the anodic (but not cathodic) {111} OH-adsorption feature at $+0.1\ V$, and suppressed current density (both anodic and cathodic) between $+0.35\ V < E < +0.50\ V$. Here, the suppressed charge for $E > +0.35\ V$ denotes, from a concerted electrochemical and copper-centric perspective, a decrease in the total number of electrochemically addressable copper sites, considering every type of site contributes charge somewhere in this region. Although certain situations involving surface restructuring might lead to an overall decrease in number of active sites (see supporting information), they are unlikely.

Reasonably, if surface morphology is indeed changing to the degree as reported in literature, one would expect to see certain types of sites increase in relative abundance with other types of sites decreasing in abundance, whilst simultaneously observing an increase in the total number of surface sites as changes in morphology bring about a shift in the site distribution and furthermore lead to (reportedly) overall smaller surface deposits. Exactly such behavior can be seen in e.g., Figure 5.2d where irreversible oxidation and reduction results in changes in relative site abundances and (for increasingly positive oxidation potentials) increases in overall surface area. However, this 'common sense' scenario is in disagreement with the voltammetry results in Figure 5.4a.

Increasing the reaction time to $60\ min$ ($-1.75\ V, 10\ M$ NaOH, Figure 5.4b) provides us with additional information: all CV changes observed for 5 and $15\ minutes$ become more prominent after $60\ minutes$, although suppression of the anodic feature at $+0.1\ V$ cannot be ascertained since this region is now masked by new features that develop. These additional features comprise, specifically, three new anodic peaks at ca. $-0.125\ V, +0.05\ V$ and $+0.2\ V$, and two new cathodic features near $+0.1\ V$ and $-0.1\ V$ (where the latter is actually a convolution of two peaks). The locations of these new features do not match with where the various types of possible copper sites are known to adsorb, considering that a Cu(poly) surface contains all kinds of possible sites and yet these newly developing features do not match in their location with any of the adsorption features observed for such a surface. Neither does their asymmetrical nature agree with the reversibility of OH adsorption on copper sites. Interestingly, when we use cyclic voltammetry to investigate what happens to a polycrystalline copper surface under CO2RR-representative conditions ($60\ min$ at $-0.75\ V$ in $0.5\ M$ KHCO$_3$ + CO$_2$ (g), Figure 5.4c), similar CV behavior is observed as after $60\ min$ at $-1.75\ V$ in $10\ M$ NaOH, though less pronounced. We also found the same behavior in less concentrated bicarbonate electrolyte ($-0.75\ V$
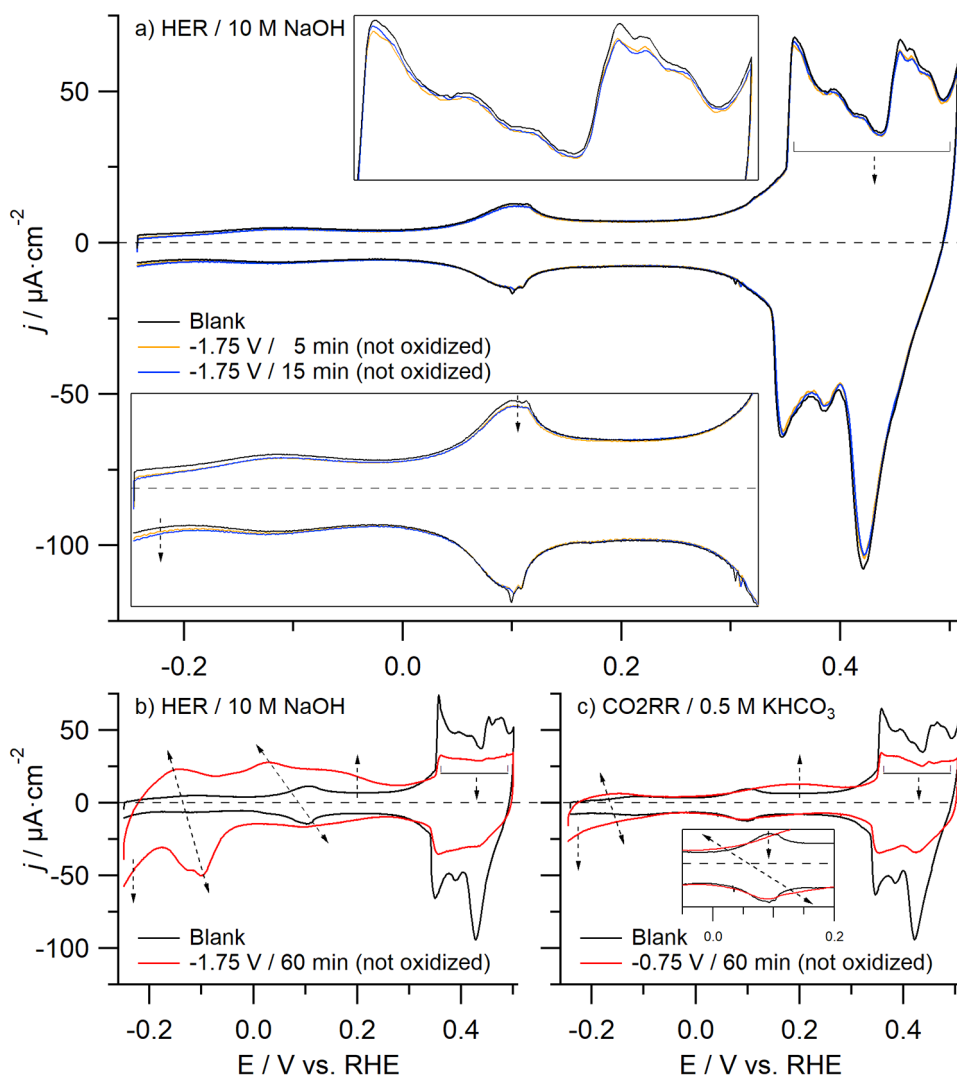
Figure 5.4: Changes in the characterization CVs ($0.1\ M$ NaOH, $v = 50\ mV \cdot s^{-1}$) of Cu(poly) surfaces after being subjected to purely cathodic conditions ($5 - 60\ min$) under various conditions. In panels a) and b) the CVs obtained after cathodization at $-1.75\ V$ in $10\ M$ NaOH for 5 (orange) and $15\ minutes$ (blue), and after $60\ minutes$ (red), are compared to their respective blank CVs ($0.1\ M$ NaOH, $v = 50\ mV \cdot s^{-1}$) (black). In panel c) the characterization CVs ($0.1\ M$ NaOH, $v = 50\ mV \cdot s^{-1}$) obtained before (blank, in black) and after (red) $60\ minutes$ of CO_2 reduction at $-0.75\ V$ in $0.5\ M$ KHCO$_3$ are depicted. Reported potentials are 85% iR corrected.

in 0.1 M KHCO$_3$, Figure D.3) for various reaction times, with CV changes already evident within 1 min and becoming more pronounced with increased reaction duration. This apparent independence on reaction conditions was further verified from CV studies after performing CO reduction in 10 M NaOH at both -0.75 V and -0.40 V (Figures D.4 and D.5, respectively) for reaction times between 1 and 30 min (e.g., comparable conditions to Figures 5.1d and 5.4a). Also in this instance, near-identical CV trends were observed after reaction in the absence and presence of CO, irrespective of the exact applied potential (-1.75 V vs. -0.75 V and -0.40 V). Namely, an absence of change in voltammetry after 1 min, and CV suppression effects plus increased HER after extended reaction duration.

In summary, voltammetric studies for longer timeframes ($5-60$ min) under various different reaction conditions resulted in comparable CV trends. Specifically, studies employing strong (-1.75 V, without CO) and weak (-0.75 V and -0.40 V, with CO) cathodic potentials in 10 M NaOH showed independence of the potential and presence of CO. Similar results (apparent independence of exact reaction conditions) were also obtained when investigating reduction (-0.75 V) in different concentrations of bicarbonate electrolyte: 0.1 M and 0.5 M KHCO$_3$. Because of the similar voltammetry results obtained under these various conditions, which were furthermore difficult to reconcile with the expected behavior of clean copper, we started doubting the applicability of this CV-centric approach for studying copper stability for extended-duration experiments.

To verify if the voltammetric data was representative of changing copper morphology or otherwise, extended-time control experiments that did not rely on CV were performed by conducting identical-location SEM studies on a micro-roughened copper surface prior to- and after 60 min of CO2RR at -0.75 V in 0.5 M KHCO$_3$. Taking into consideration the considerable changes observed in voltammetry after 60 $minutes$ of cathodization (both in 10 M NaOH and 0.5 M KHCO$_3$, Figures 5.4b and 5.4c) we would reasonably expect to be able to see such changes via SEM, if indeed the changes in voltammetry are representative of the redistribution of copper sites at the interface resulting from changing morphology. E.g., CV changes of similar magnitude were observed in Figure 5.2d, and resulted in easily identifiable roughening in the SEM (Figure 5.3). The basis for this study was an anisotropically (Figure D.2) roughened spherical single crystal (halide-induced roughening procedure described in the experimental section) that retained its macroscopic anisotropy resulting from its initial single-crystallinity but exhibited facet-dependent nanoscale morphology after roughening.

After the roughening procedure, the crystal was rinsed and dried under reducing atmosphere and moved to the SEM, where multiple easily identifiable spots of various morphologies were imaged. Next, it was transferred to the electrochemical setup where it was subjected to -0.75 V in 0.5 M KHCO$_3$ for 60 min under constant CO$_2$ bubbling. Deactivation on this timescale for this electrode is evident from the current response of the system (Figure D.6). Copper-catalyst deactivation under similar conditions; ca. 1 $hour$ of CO2RR at potentials between -1 $V < E < -0.7$ V in bicarbonate electrolyte between 0.1 M and 0.5 M for both unpurified and pre-purified electrolytes has also been observed by other authors. E.g., see current

traces reported by Kuhl *et al.*[34], Wang *et al.*[35], and Wuttig *et al.*[7] Additionally, Popovic *et al.*[10] write about the morphological evolution of copper on a similar timescale and under similar conditions (i.e., $50\ min$ at $-0.70\ V$ in $0.1\ M$ KHCO$_3$). After conducting CO2RR, the electrode was rinsed, dried and moved to the SEM once again. As described in a previous section (accompanying Figure 5.3), the crystal was manually positioned to match as best as possible its previous orientation using the surface anisotropy. Because of this manual step, the incidence angle of the electron beam with respect to the surface normal will deviate slightly between the two datasets, with this mismatch being exacerbated by the curvature of the surface. Previously imaged sites were re-located and a follow-up set of micrographs was taken for each location.

The results of this experiment are shown in Figure 5.5, where micrographs of various spots on the surface exhibiting different morphologies on the mesoscale (ca. $50-200\ nm$ range) obtained before (left-hand side) and after (right-hand side) CO2RR are depicted. Mesoscale surface stability after one hour of reaction time can be investigated by comparing Figures 5.5a, c, e, and g with Figures 5.5b, d, f, and h for micrographs of the surface prior to- and after CO2RR, respectively. Insets show a magnification of a region located within the associated full-sized images. The discussion for this particular experiment is straightforward: the surface was found to be virtually unchanged to within the detection limits for our system. Overall shapes and locations of the variously sized and oriented microparticles located in these images remain static. If anything, there can be observed one difference between Figures 5.5e and 5.5f; an additional particle being located near the bottom-middle for Figure 5.5f, which we believe is likely dust. Though the resolution of the SEM is limited, a copper surface is commonly believed to undergo signification changes under CO2RR conditions on the length-scale we investigate and should be easily visible in the insets provided in Figure 5.5.[21] However, as we are very careful to minimize surface oxidation at every step of the experiment, we find that deposits tens of nanometers in size (i.e., highly reactive and therefore unstable) exhibit high stability within the timeframe and resolution of our system.

Although SEM is incapable of resolving the (distribution of) facets at the interface (one would need atomically resolved and preferably in-situ techniques for such information), CV evidence (which is structure sensitive) for short timeframes under cathodic conditions in $10\ M$ NaOH on the three basal planes and defect-rich polycrystalline copper indicated no discernible surface changes, which is in good qualitative agreement with the SEM data provided in both Figure 5.3 ($5\ min$ at $-1.75\ V$ in $10\ M$ NaOH) and Figure 5.5 ($60\ min$ at $-0.75\ V$ in $0.5\ M$ KHCO$_3$), as also there we observe no morphological differences to within the limits of our instrument in absence of surface oxidation. However, the SEM data in Figure 5.5 evidently disagrees with the CV data obtained for such longer time periods (Figure 5.4c), based on which we would expect, at a minimum, identifiable change in morphology on the ca. $50\ nm$ scale, if indeed the CV evolution is representative of a changing distribution of facets at the interface. From these results, we believe that the cyclic voltammetry results obtained after $5 - 60\ minutes$ of reduction are not related to changes in surface morphology as induced by the negative interfacial potential.
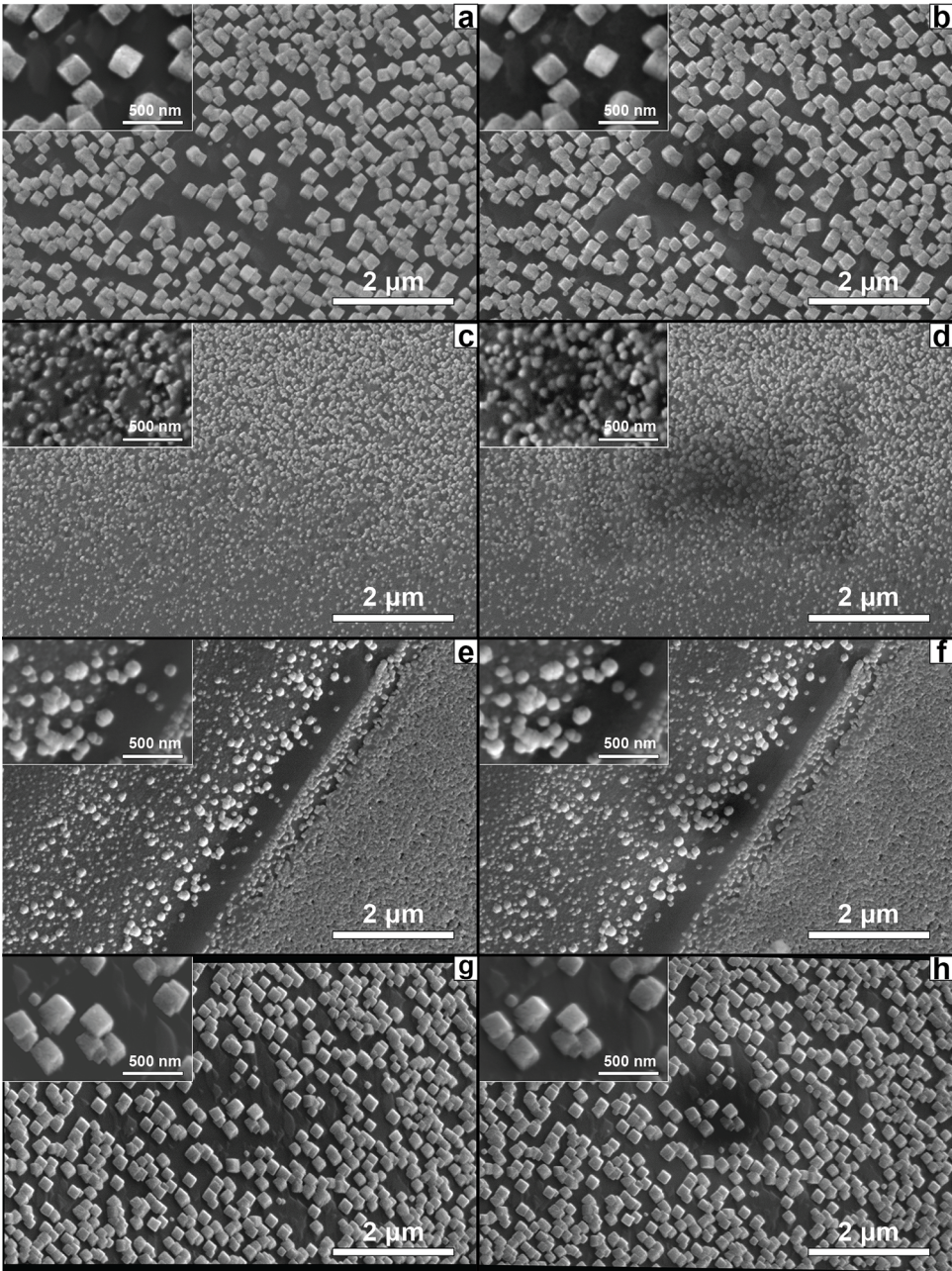
Figure 5.5: Identical location SEM of an electrochemically roughened spherical single crystal electrode before (left-hand: a, c, e and g) and after (right-hand: b, d, f and h) $60\ min$ of CO2RR at $-0.75\ V$ vs. RHE in $0.5\ M$ KHCO$_3$ for various locations on the crystal.

Neither can we attribute the observed CV trends to unintended oxidation, considering the behavior is very different from the changes we see when comparing CVs obtained for pre-oxidized surfaces (Figure 5.2) and cathodic-only treated surfaces (Figure 5.1). Hence, we posit that the changes in voltammetry after extended reaction duration must be related to something other than cathodically induced and/or anodically induced morphological surface evolution. We suggest the changes may instead be related to the blocking of copper sites with foreign species, as that would agree with the appearance of non-copper features in the CV which become more prominent as a function of time, together with the suppression of adsorption charge of known copper sites.
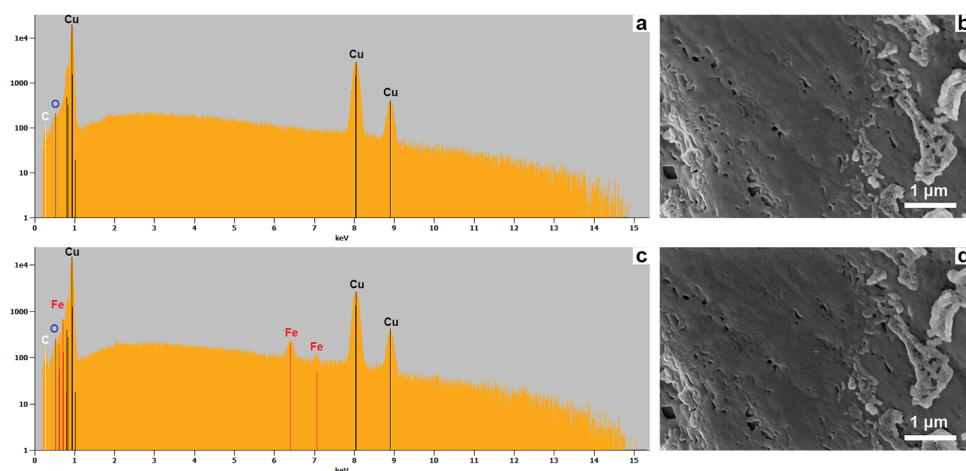
Figure 5.6: Surface morphology and elemental analysis results before and after ca. $5\ hours$ of CO2RR at $-0.75\ V$ in saturated $KHCO_3$ solution under constant CO_2 (g) purging for an arbitrary location on a nitric acid-cleaned polycrystalline bead electrode. Panels a) and c) show the EDX spectrum obtained prior to- and after CO2RR whilst b) and d) show the accompanying SEM micrographs for where EDX was performed.

To investigate this hypothesis, we conducted the following experiment. Firstly, a Cu(poly) bead-type electrode was grown and cleaned as per steps (a-c) of single crystal growth described in the experimental. After a final HNO_3 etching and Milli-Q rinsing step, it was not remolten. Rather it was briefly (ca. $10\ s$) annealed inductively in pure hydrogen to remove the oxide layer, but at much lower temperatures than used normally (i.e., decreased instrument power) so as to prevent migration of bulk contaminants to the surface. The crystal was cooled down in hydrogen, moved to the SEM and had its elemental composition investigated via energy-dispersive X-ray spectroscopy (EDX) for various locations to verify that the surface was devoid of contaminants to within the accuracy of the apparatus. Thereafter, the crystal was moved to our controlled-atmosphere electrochemical setup and CO2RR was carried out in saturated $KHCO_3$ solution (with sufficient $KHCO_3$ added to nominally reach $2\ M$) under constant CO_2 bubbling at $-0.75\ V$ for ca. $5\ hours$. Finally, the surface was rinsed under reducing conditions, dried in hydrogen, and moved back to the

SEM where EDX was performed once more. Results representative of the overall observed behavior are depicted in Figure 5.6 with additional locations provided in Figures D.7 and D.8.

Although more convincing proof and a more detailed discussion of the morphological stability of copper is provided in the previous section, the respective micrographs in shown Figures 5.6b and 5.6d (before and after CO2RR, respectively) agree with those data: little to no change in surface morphology can be seen. However, elemental analysis shows a different story; with EDX showing no Fe prior to CO2RR (Figure 5.6a) but iron being clearly visible after (Figure 5.6c). Identical observations were made for various regions on the crystal located hundreds of μm apart and having differing morphologies (see e.g., Figures D.7 and D.8), all exhibiting no distinguishable changes in morphology but with traces of iron present after the experiment. Hence, we believe that the changes in cyclic voltammetry that we observe when reaction time is increased (Figure 5.4) are most probably related to fouling by solution impurities rather than changes in the distribution of facets at the surface resulting from morphological evolution.

5.4. Conclusions

The cathodic stability of the various principal surfaces of copper, together with a defect-rich polycrystalline surface, was investigated under known highly cathodically corrosive conditions[13, 23] as well as under commonplace CO2RR conditions. The stability of these surfaces was found to be exquisite under purely cathodic potentials, so-long as oxide formation was entirely avoided (Figure 5.1). However, allowing the surface to partially oxidize resulted in rapid changes in the distribution of active sites at the surface (Figure 5.2). The morphological stability under cathodic-only conditions for both HER at $-1.75\ V$ in $10\ M$ NaOH and CO2RR at $-0.75\ V$ in $0.5\ M$ KHCO$_3$ + CO$_2$ (g) for prolonged times was corroborated by SEM, with no surface roughening observed to within the accuracy of the equipment for both instances when surface oxidation was absent (Figures 5.3 and 5.5, respectively). Voltammetric data after such prolonged reaction times (Figure 5.4) proved to be unreliable, showing very different behavior from CV results obtained for shorter periods of time (Figure 5.1, no changes), exhibiting instead the development of features unrelated to copper, where various different electrolytes and reaction conditions all yielded comparable results. We show that the mismatch between CV data and SEM data after cathodization for extended periods of time is related to electrode fouling as determined via SEM+EDX, where surface morphology was found static but elemental analysis showed iron to be present after reaction (Figure 5.6 and Figures D.7/D.8).

Our findings are in contradiction with current literature, wherein it is often proposed that the catalyst deactivation observed for Cu surfaces is possibly due to changes in surface morphology resulting in facet redistribution[12, 14, 19–21, 36], as induced in some manner by the reaction environment (e.g., due to the applied potential[12, 16, 17], or due to (CO2RR intermediate-related) adsorbates[37], or due to the local pH[36, 38], or other factors). However, a comparatively much simpler explanation underlying reported changes in surface morphology exists: acci-

dental surface oxidation and subsequent anisotropic (Figures 5.2 and 5.3) reduction of the surface (likely in concert with dissolution and redeposition) as also proposed by Popovic *et al.*[10], where the rate of reduction of these oxides is likely to influence the final morphology. Such unintended (partial) surface oxidation is easily achieved, considering that the open circuit potential for copper falls within the region where surface oxidation takes place[11] and with increasingly complicated setups becoming more prevalent, increasing also the likelihood of minor experimental errors. In agreement with this theory, we show that brief oxidation ($1\ min$) at potentials very close to the open circuit potential of copper ($+0.50\ V$ vs. RHE), resulted in appreciable differences in cyclic voltammetry (Figure 5.2) denoting anisotropic surface restructuring. Thus, we conclude that oxidation-reduction cycles are at the basis of the reported morphological changes for copper, with the thickness of such (accidentally formed) oxide layers, their subsequent (rate of) reduction, and the number of such oxidation/reduction cycles yielding the various (changes in) morphologies reported. This agrees well with Speck and Cherevko[11] who report the absence of copper dissolution at negative potentials down to $-1\ V$ vs. RHE, stating: *"...but further oxidation at open circuit potential results in dissolution."*

As a final consideration we would like to point out that the conclusions we draw in this work may contradict with conclusions of other authors on this topic, however the data we base our (and others their) conclusions on are not necessarily in disagreement with other data. This is best illustrated by two recent works by Simon *et al.*[12], and by Popovic *et al.*[10] In the former, in-situ EC-AFM images are presented showing that a Cu(100) surface imaged at open circuit in $0.1\ M$ KHCO$_3$ changes its morphology once CO2RR conditions are applied, with the resulting surface morphology being a function of the applied potential. However, it is also stated that *"...[We] performed CO2RR... over extended periods of time [..., but AFM] images reveal no obvious morphological changes on the surface over the reaction times studied..."*.[12] Hence, the change in morphology occurred after stepping from open circuit to their potential of interest, which agrees well with our proposed mechanism of oxidation-induced morphological change, which in the case of Simon *et al.*[12] would be the result of starting at open circuit potential. Similarly, Popovic *et al.*[10] show degradation of a ca. $500\ nm$ radius Cu nanoparticle, but their study also contains periods at open circuit translating to successive oxidation and reduction cycles. In our work we employ extremely cathodic potentials, resulting in the electrolyte near the surface being supersaturated with hydrogen when we disconnect the electrical circuit. Thereafter, we rinse briefly under strong hydrogen flow and dry our electrodes in an isolated environment under high hydrogen flow. Hence, we minimize such oxidation that would occur at open circuit potentials, and can show that the CV does not change after brief periods of cathodization. Though contamination effects prohibit us from providing the same type of proof for prolonged periods of time, identical location SEM measurements serve to show that the morphology is stable, at least on the length-scale reported on by Popovic *et al.*[10]

References

[1] Matthew Jouny, Wesley Luc, and Feng Jiao. General techno-economic analysis of CO2 electrolysis systems. *Industrial & Engineering Chemistry Research*, 57(6):2165–2177, 2018.

[2] Md Golam Kibria, Jonathan P. Edwards, Christine M. Gabardo, Cao-Thang Dinh, Ali Seifitokaldani, David Sinton, and Edward H. Sargent. Electrochemical CO2 reduction into chemical feedstocks: From mechanistic electrocatalysis models to system design. *Advanced Materials*, 31(31):1807166, 2019.

[3] Jared Sisler, Shaihroz Khan, Alexander H. Ip, Moritz W. Schreiber, Shaffiq A. Jaffer, Erin R. Bobicki, Cao-Thang Dinh, and Edward H. Sargent. Ethylene electrosynthesis: A comparative techno-economic analysis of alkaline vs membrane electrode assembly vs CO2–CO–C2H4 tandems. *ACS Energy Letters*, 6(3):997–1002, 2021.

[4] Jun Tae Song, Hakhyeon Song, Beomil Kim, and Jihun Oh. Towards higher rate electrochemical CO2 conversion: From liquid-phase to gas-phase systems. *Catalysts*, 9(3):224, 2019.

[5] Sumit Verma, Byoungsu Kim, Huei-Ru "Molly" Jhong, Sichao Ma, and Paul J. A. Kenis. A gross-margin model for defining technoeconomic benchmarks in the electroreduction of CO2. *ChemSusChem*, 9(15):1972–1979, 2016.

[6] Y. Hori, H. Konishi, T. Futamura, A. Murata, O. Koga, H. Sakurai, and K. Oguma. "deactivation of copper electrode" in electrochemical reduction of CO2. *Electrochimica Acta*, 50(27):5354–5369, 2005.

[7] Anna Wuttig and Yogesh Surendranath. Impurity ion complexation enhances carbon dioxide reduction catalysis. *ACS Catalysis*, 5(7):4479–4484, 2015.

[8] David W. DeWulf, Tuo Jin, and Allen J. Bard. Electrochemical and surface studies of carbon dioxide reduction to methane and ethylene at copper electrodes in aqueous solutions. *Journal of The Electrochemical Society*, 136(6):1686–1691, 1989.

[9] Dan Ren, Nian Tee Wong, Albertus Denny Handoko, Yun Huang, and Boon Siang Yeo. Mechanistic insights into the enhanced activity and stability of agglomerated Cu nanocrystals for the electrochemical reduction of carbon dioxide to n-propanol. *Journal of Physical Chemistry Letters*, 7(1):20–24, 2016.

[10] Stefan Popovic, Marjan Bele, and Nejc Hodnik. Reconstruction of copper nanoparticles at electrochemical CO2 reduction reaction conditions occurs via two-step dissolution/redeposition mechanism. *ChemElectroChem*, (DOI: 10.1002/celc.202100387), 2021.

[11] Florian D. Speck and Serhiy Cherevko. Electrochemical copper dissolution: A benchmark for stable CO2 reduction on copper electrocatalysts. *Electrochemistry Communications*, 115:106739, 2020.

[12] Georg H. Simon, Christopher S. Kley, and Beatriz Roldan Cuenya. Potential-dependent morphology of copper catalysts during CO2 electroreduction revealed by in-situ atomic force microscopy. *Angewandte Chemie International Edition*, 60(5):2561–2568, 2021.

[13] Alexei I. Yanson, Paramaconi Rodriguez, Nuria Garcia-Araez, Rik V. Mom, Frans D. Tichelaar, and Marc T. M. Koper. Cathodic corrosion: A quick, clean, and versatile method for the synthesis of metallic nanoparticles. *Angewandte Chemie International Edition*, 50(28):6346–6350, 2011.

[14] Youn-Geun Kim, Jack Hess Baricuatro, Alnald Javier, John Mathew Gregoire, and Manuel P. Soriaga. The evolution of the polycrystalline copper surface, first to Cu(111) and then to Cu(100), at a fixed CO2RR potential: A study by operando EC-STM. *Langmuir*, 30(50):15053–15056, 2014.

[15] Hisayoshi Matsushima, Andriy Taranovskyy, Christian Haak, Yvonne Gründer, and Olaf M. Magnussen. Reconstruction of Cu(100) electrode surfaces during hydrogen evolution. *Journal of the American Chemical Society*, 131(30):10362–10363, 2009.

[16] Thanh Hai Phan, Karla Banjac, Fernando P. Cometto, Federico Dattila, Rodrigo García-Muelas, Stefan J. Raaijman, Chunmiao Ye, Marc T. M. Koper, Núria López, and Magalí Lingenfelder. Emergence of potential-controlled Cu-nanocuboids and graphene-covered Cu-nanocuboids under operando CO2 electroreduction. *Nano Letters*, 21(5):2059–2065, 2021.

[17] Beatriz Roldán Cuenya, Fabian Scholten, Khanh-Ly C. Nguyen, Jared P. Bruce, and Markus Heyde. Identifying structure-selectivity correlations in the electrochemical reduction of CO2: comparison of well-ordered atomically-clean and chemically-etched Cu single crystal surfaces. *Angewandte Chemie International Edition*, (DOI: 10.1002/anie.202103102), 2021.

[18] Rosa M. Arán-Ais, Fabian Scholten, Sebastian Kunze, Rubén Rizo, and Beatriz Roldan Cuenya. The role of in situ generated morphological motifs and Cu(i) species in C2+ product selectivity during CO2 pulsed electroreduction. *Nature Energy*, 5(4):317–325, 2020.

[19] Youn-Geun Kim, Jack H. Baricuatro, and Manuel P. Soriaga. Surface reconstruction of polycrystalline Cu electrodes in aqueous KHCO3 electrolyte at potentials in the early stages of CO2 reduction. *Electrocatalysis*, 9(4):526–530, 2018.

[20] Youn-Geun Kim, Alnald Javier, Jack H. Baricuatro, Daniel Torelli, Kyle D. cummins, Chu F. Tsang, John C. Hemminger, and Manuel P. Soriaga. Reprint

of: Surface reconstruction of pure-Cu single-crystal electrodes under CO-reduction potentials in alkaline solutions: A study by seriatim ECSTM-DEMS. *Journal of Electroanalytical Chemistry*, 793:113–118, 2017.

[21] Stefan Popović, Milutin Smiljanić, Primož Jovanovič, Jan Vavra, Raffaella Buonsanti, and Nejc Hodnik. Stability and degradation mechanisms of copper-based catalysts for electrochemical CO2 reduction. *Angewandte Chemie International Edition*, 59(35):14736–14746, 2020.

[22] Thomas J. P. Hersbach, Alexei I. Yanson, and Marc T. M. Koper. Anisotropic etching of platinum electrodes at the onset of cathodic corrosion. *Nature Communications*, 7:12653, 2016.

[23] A. I. Yanson, P. V. Antonov, P. Rodriguez, and M. T. M. Koper. Influence of the electrolyte concentration on the size and shape of platinum nanoparticles synthesized by cathodic corrosion. *Electrochimica Acta*, 112:913–918, 2013.

[24] Thomas J. P. Hersbach, Ian T. McCrum, Dimitra Anastasiadou, Rianne Wever, Federico Calle-Vallejo, and Marc T. M. Koper. Alkali metal cation effects in structuring Pt, Rh, and Au surfaces through cathodic corrosion. *ACS Applied Materials & Interfaces*, 10(45):39363–39379, 2018.

[25] Thomas J. P. Hersbach, Vladislav A. Mints, Federico Calle-Vallejo, Alexei I. Yanson, and Marc T. M. Koper. Anisotropic etching of rhodium and gold as the onset of nanoparticle formation by cathodic corrosion. *Faraday Discussions*, 193(0):207–222, 2016.

[26] Stefan J. Raaijman, Nakkiran Arulmozhi, and Marc T. M. Koper. Anisotropic cathodic corrosion of gold electrodes in the absence and presence of carbon monoxide. *Journal of Physical Chemistry C*, 124(52):28539–28554, 2020.

[27] S.J. Raaijman, N.Arulmozhi, and M.T.M.Koper. Clean and reproducible voltammetry of copper single crystals with prominent facet-specific features using induction annealing. (manuscript submitted for publication), 2021.

[28] Nakkiran Arulmozhi and Gregory Jerkiewicz. Design and development of instrumentations for the preparation of platinum single crystals for electrochemistry and electrocatalysis research. Part 1: Semi-automated crystal growth. *Electrocatalysis*, 7(6):507–518, 2016.

[29] F. Sloan Roberts, Kendra P. Kuhl, and Anders Nilsson. High selectivity for ethylene from carbon dioxide reduction over copper nanocube electrocatalysts. *Angewandte Chemie*, 127(17):5268–5271, 2015.

[30] Paula Sebastián-Pascual, Francisco J. Sarabia, Víctor Climent, Juan M. Feliu, and María Escudero-Escribano. Elucidating the structure of the Cu-alkaline electrochemical interface with the laser-induced temperature jump method. *The Journal of Physical Chemistry C*, 2020.

5

[31] Aarti Tiwari, Hendrik H. Heenen, Anton Simon Bjørnlund, Degenhart Hochfilzer, Karen Chan, and Sebastian Horch. Electrochemical oxidation of CO on Cu single crystals under alkaline conditions. *ACS Energy Letters*, 5(11):3437–3442, 2020.

[32] Klaas Jan P. Schouten, Elena Pérez Gallent, and Marc T.M. Koper. The electrochemical characterization of copper single-crystal electrodes in alkaline media. *Journal of Electroanalytical Chemistry*, 699:6–9, 2013.

[33] Nakkiran Arulmozhi, Derek Esau, Ram P. Lamsal, Diane Beauchemin, and Gregory Jerkiewicz. Structural transformation of monocrystalline platinum electrodes upon electro-oxidation and electro-dissolution. *ACS Catalysis*, 8(7):6426–6439, 2018.

[34] Kendra P. Kuhl, Etosha R. Cave, David N. Abram, and Thomas F. Jaramillo. New insights into the electrochemical reduction of carbon dioxide on metallic copper surfaces. *Energy & Environmental Science*, 5(5):7050–7059, 2012.

[35] Lei Wang, Stephanie A. Nitopi, Erlend Bertheussen, Marat Orazov, Carlos G. Morales-Guio, Xinyan Liu, Drew C. Higgins, Karen Chan, Jens K. Nørskov, Christopher Hahn, and Thomas F. Jaramillo. Electrochemical carbon monoxide reduction on polycrystalline copper: Effects of potential, pressure, and pH on selectivity toward multicarbon and oxygenated products. *ACS Catalysis*, 8(8):7445–7454, 2018.

[36] Wei Luo, Lei Hu, Yimin Xv, Jian Zhou, Wentao Xv, and Mi Yan. Electrochemical corrosion behavior and surface passivation of bulk nanocrystalline copper in alkaline solution. *Anti-Corrosion Methods and Materials*, 2020.

[37] Phil De Luna, Rafael Quintero-Bermudez, Cao-Thang Dinh, Michael B. Ross, Oleksandr S. Bushuyev, Petar Todorović, Tom Regier, Shana O. Kelley, Peidong Yang, and Edward H. Sargent. Catalyst electro-redeposition controls morphology and oxidation state for selective carbon dioxide reduction. *Nature Catalysis*, 1(2):103–110, 2018.

[38] Yaran Zhao, Xiaoxia Chang, Arnav S. Malkani, Xuan Yang, Levi Thompson, Feng Jiao, and Bingjun Xu. Speciation of Cu surfaces during the electrochemical CO reduction reaction. *Journal of the American Chemical Society*, 142(21):9735–9743, 2020.